





Improved wear, mechanical, and biological behavior of UHMWPE-HAp-zirconia hybrid nanocomposites with a prospective application in total hip joint replacement

Meysam Salari¹ , Sara Mohseni Taromsari¹ , Reza Bagheri^{1,*} , and Mohammad Ali Faghihi Sani¹ 

¹ Polymeric Materials Research Group (PMRG), Department of Materials Science and Engineering, Sharif University of Technology, P.O. Box 11155-9466, Tehran, Iran

Received: 8 September 2018

Accepted: 13 November 2018

Published online:
21 November 2018

© Springer Science+Business Media, LLC, part of Springer Nature 2018

ABSTRACT

Medical engineering advances in total joint replacements and societies' rising demand for long-lasting materials have proven it essential to manufacture materials that are more similar to the original tissue in the fields of mechanical, tribological, and biological properties. Ultra-high molecular weight polyethylene (UHMWPE) is a polymer widely used in arthroplasty applications due to its biocompatibility, chemical stability, and reasonable mechanical properties; however, it still fails to entirely meet the standards of the hip joint implant. In this study, different concentrations of nanosized zirconia were added to UHMWPE and HAp matrix with an intended application in arthroplasty. Liquid-phase ultrasonication and hot pressing were employed to disperse the reinforcing phases and to form the final standard samples, respectively. Tensile, Vickers hardness, and pin-on-disk tests were carried out to evaluate mechanical and wear properties of the samples. In the meanwhile, *in vitro* biological properties were studied via MTT assay, alkaline phosphatase enzyme activity, and cell morphology tests. Dispersion features, microstructural structures, and cell adhesion were also assessed using scanning electron microscopy (SEM). Results indicate improvement in both tensile and wear properties by zirconia addition; for instance, the sample containing 10 wt% zirconia and 10 wt% HAp exhibits 45% increase in yield strength and 64% reduction in coefficient of friction. On the other hand, biological properties have also significantly improved with zirconia incorporation, at which all samples proved to be biocompatible with an increase in both osteoblasts activity and cell adhesion with increasing zirconia concentration.

Address correspondence to E-mail: rezabagh@sharif.edu

Introduction

Human hip joint is predominantly considered as the most important joint due to the variety of movement capabilities and the load-bearing requirements which vary under different activities [1]. This leads to the joint vulnerability and its proneness to injury following cartilage damage, abrasion, arthritis, and fractures and eventually results in patients not being able to continue their routine life, at which the necessity of arthroplasty lies beneath [1, 2]. Therefore, total hip joint replacement is considered as the most successful achievement of orthopedic sciences in the past decades [1, 2]. A total hip joint implant consists of a femoral head, a femoral stem, and an acetabular cup which are mostly made of metals such as stainless steel and titanium alloys, or of ceramics such as zirconia and alumina [3, 4]. Thus, the repetitive and constant abrasion between the two metal–metal or metal–ceramic components could result in the generation of cytotoxic metallic wear debris [3, 4]. In order to overcome this obstacle, a plastic liner or socket is added to prevent the abrasion between the two femoral and acetabular components [3–5]. These plastic components are mostly made of ultra-high molecular weight polyethylene (UHMWPE), which is a medical-grade polymer showing appropriate mechanical properties as well as chemical and biological stability in comparison to other plastics [6]. However, still the coefficient of friction, surface hardness and wear resistance of this polymer are not sufficient enough for such prospective application [6]. Wear debris can significantly damage joint replacements by activating osteoclasts which resorb the bone surrounding the implant in a process named osteolysis which itself is known as the main phenomenon of implants failure [7]. Moreover, insufficient yield strength of UHMWPE can result in permanent deformation and failure at high contact stress [8]. On the other hand, one of the key factors needed to be considered for a successful implant is its biocompatibility and cytotoxicity that is caused by the implants, which would also cause adverse biological responses and eventual implant failure. Tribological, biological, and mechanical drawbacks of hip implants are summarized in Fig. 1.

Consequently, efforts have been put on to improve mechanical properties of UHMWPE sockets [6, 9]. Along this line, incorporation of inorganic fillers to overcome shortcomings of the UHMWPE matrix

seems to be a promising solution [9, 10]. Despite the reinforcing effect of these fillers, there are still some drawbacks that ought to be considered, including the high level of loading of these fillers needed to provide the acceptable mechanical properties. For instance, some investigations have employed 50 wt% of hydroxyapatite [11, 12], 40 wt% of micro-sized zirconia [13] and 24 wt% of kaolin [14] to achieve the desired properties. The researchers carried out these studies have all used considerable amount of the reinforcing particles, 40 wt% or more, in order to enhance the deficit in mechanical and tribological properties of the neat UHMWPE sockets. With an emphasis on retaining the desired properties should be retained by adding the minimum possible amount of the reinforcements, the goal of the current study is to incorporate two ceramic fillers in a UHMWPE matrix in the form of a hybrid composite to obtain reasonable mechanical properties at lower portion of reinforcement. Considering the positive reports on the use of nanoreinforcements [11–18], nanopowder of hydroxyapatite (HAp) and zirconium oxide were selected for this purpose. HAp has proven to maintain an appropriate level of biocompatibility as with a chemical structure of $\text{Ca}_{10}(\text{PO}_4)_6(\text{OH})_2$, it has a Ca/P value of about 1.67, which is similar to that of natural bone [11, 15]. On the other hand, zirconia is widely used in prosthetic devices due to its good mechanical properties including hardness, yield strength, modulus of elasticity, and wear resistance as well as being resistant in aggressive environments and bioinertness [16]. Ultrasonication in liquid phase followed by hot pressing to form the final hybrid nanocomposites [17, 18] is employed as a rather simple method for synthesizing the samples. Tensile, hardness, and wear resistance of the samples have been examined in this study. Morphology of the samples has been analyzed via scanning electron microscopy (SEM). Biological performance of the samples was evaluated through MTT assay, cell morphology, and alkaline phosphatase (ALP) enzyme level using MG-63 osteoblast cells. In all three categories, hybrid nanocomposites proved to be effective in achieving the desired properties, coming to a conclusion that the resulted material might find a prospective application in artificial joint replacement.

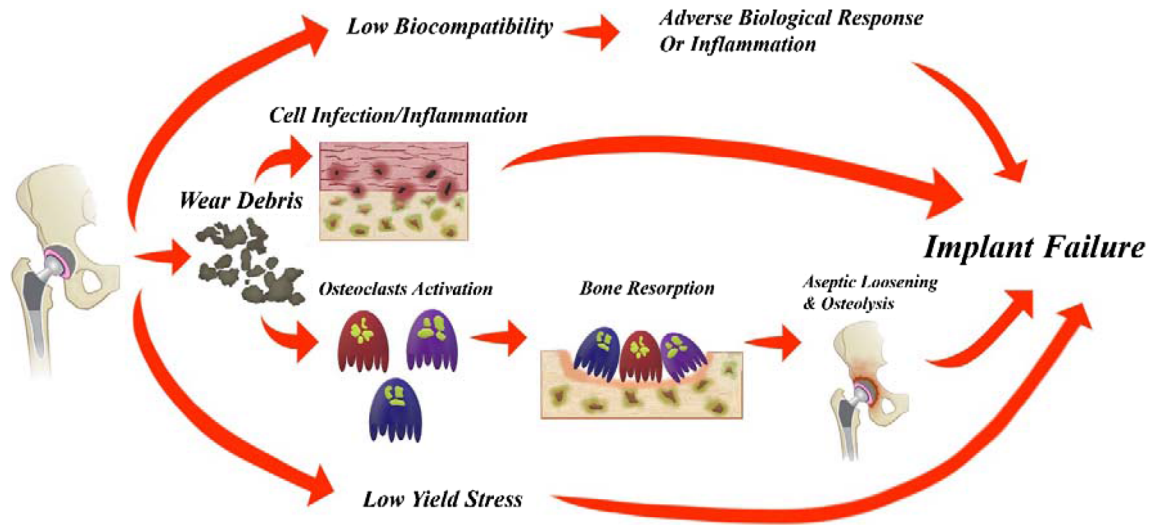


Figure 1 Mechanical, tribological and biological drawbacks of hip implants, especially UHMWPE liners.

Experimental

Materials

UHMWPE powder with an average molecular weight of 6×10^6 g/mol (with density of 0.94 g/mL at 25 °C, and CAS number 429015) and zirconium oxide powder (nanopowder < 100 nm (TEM) and density of 5.89 g/mL at 25 °C with CAS number 1314234) were purchased from Sigma-Aldrich. Hydroxyapatite nanopowder was synthesized through sol-gel method using analytical grade $\text{Ca}(\text{NO}_3)_2 \cdot 4\text{H}_2\text{O}$ (with CAS number 13477-34-4, Merck Millipore) and P_2O_5 (with CAS number 1314-65-3, Merck Millipore) powders. 99.9% purified ethanol (with CAS number 64-17-5, Merck Millipore) was used as a medium and Vitamin-E acetate (with CAS number 7695-91-2, Merck Millipore) was also purchased to be used as an antioxidant.

Preparation of hydroxyapatite nanopowder

According to Feng et al. [19], appropriate amounts of calcium nitrate tetrahydrate ($\text{Ca}(\text{NO}_3)_2 \cdot 4\text{H}_2\text{O}$) and phosphoric pentoxide (P_2O_5) were separately dissolved in ethanol. The two solutions were then mixed to form a solution in which the Ca/P ratio is 1.67. The mixture was then stirred for 1 h at 25 °C and then at 60 °C for 12 h to complete the gelation stage. The aging stage and final heat treatment were carried out at ambient temperature and at 650 °C for 5 h with a heating rate of 10 °C/min, respectively. The white

dried mixture was then crushed with an agate mortar and pestle (MicroFAST-1000) to obtain the nanopowder. The powder was characterized using x-ray diffraction spectroscopy (XRD JEOL, JDX-8030) with the angular range of $2\theta = 0^\circ$ to 80° using Cu-K_α radiation with $\lambda = 1.5418 \text{ \AA}$. Morphology and particle size and distribution were also examined using scanning electron microscopy (SEM: TE-SCAN, Vega).

Sample preparation

A simple method was used to prepare nanocomposite powders by means of ultrasonication and stirring in a liquid medium. For this purpose, each reinforcing phase and the UHMWPE powder were firstly weighed according to Table 1 which depicts samples formulation. It is worthful to mention that according to the literature, 10 wt% HAp is an apparent optimum amount reported to satisfy the biocompatibility and properties needed for such

Table 1 Formulation and composition of samples

Sample name	Sample composition (weight fraction)		
	UHMWPE (%)	HAp (%)	Zirconia (%)
U	100	0	0
UH	90	10	0
UHZ(2)	88	10	2
UHZ(6)	84	10	6
UHZ(10)	80	10	10

purposes, while not adversely affecting the mechanical properties [11, 12, 20, 21]. In addition, in order to evaluate zirconia incorporation, 2, 6 and 10 wt% of zirconia were added to the UHMWPE-10 wt% HAp. Secondly, each of these phases was first dispersed in 25 mL ethanol using ultrasonication for 45 min at 50 W and stirring simultaneously. The resulted mixture was then added to a UHMWPE-50 mL ethanol mixture and was ultrasonicated for another 45 min. At the next stage, the mixture was stirred for 30 min at 70 °C to extract the medium, while the stirring process prevents any precipitation. The final powder was then transferred to an oven and was heated for 48 h at 90 °C to assure complete solvent extraction. Eventually, the final dry powders were hot-pressed at 230 °C and 200 bar for 1 h and then were cooled under the same pressure to form the final testing samples. Figure 2 shows a schematic description of the sample preparation process.

Sample characterization

Mechanical properties

A tensile testing machine (Hounsfield universal H10KS) was used to evaluate tensile properties of the samples according to ASTM D638. Testing, which was conducted at a crosshead speed of 50 mm/min and a uniaxial direction with a 100-KN load cell, was repeated three times for each composition to raise the accuracy and the mean values were reported. In order to evaluate hardness of the samples, Vickers hardness test was carried out using a microhardness testing machine (Buehler, 1600-6100), which applied a load of 0.1 N for 15 s on cut samples with the surface area of 1 cm². Each sample was tested three times, and the average hardness value was reported.

Morphology and crystalline structure

In order to study microstructural properties of samples, cryogenic fracture surfaces were coated and then assessed using a SEM (TE-SCAN, Vega) operated at 15 kV. A TA-Q100 differential scanning calorimetry (DSC) instrument was also employed to study melting temperature and possible effects of reinforcing phases on crystalline structure.

Wear properties

Wear test was carried out on all samples according to ASTM G99 using a micro tribometer pin-on-disk machine (Faragir Sanat Mehrbin) to investigate the wear and friction behavior when a stainless steel pin slides against the nanocomposites surfaces under dry condition. The pin was 5 mm in diameter and was fixed on the load arm applying a load of 60 N to the sample sliding with a linear velocity of 0.214 m/s. Each sample went through the fixed testing conditions for 1 h and 20 min and a total sliding distance of 1 km. In addition to the coefficient of friction which is derived directly from the test, wear rates were also calculated using Eq. 1:

$$k = \Delta m / \rho FL \quad (1)$$

where k is the wear rate in m²/N, Δm is the weight loss in mg, ρ is the density in g/cm³, F is the applied load in N and L is the total sliding distance in m. For this matter, all samples were weighed before and after the test. Besides, small disks with 10 mm in diameter and 3 mm in thickness were fabricated, and then densities were calculated measuring accurate weight and volume of each sample. Besides, each sample was measured three times and the average values were reported.

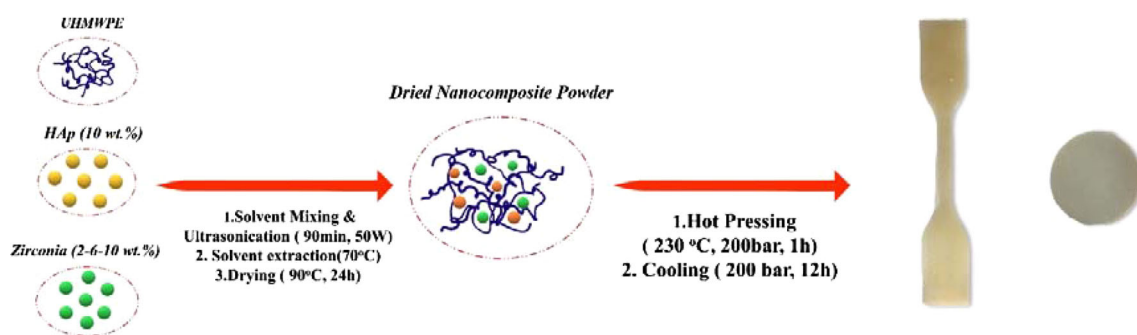


Figure 2 Schematic description of sampling process used to prepare testing samples.

Biological tests: cell culture and seeding

All three biological tests were conducted according to ISO 10993-12 in Pasteur Institute of Iran [11]. The human primary osteogenic sarcoma cell line MG-63 Colon A141B1 were used for these tests and were cultured in Dulbecco's modified Eagle medium (DMEM; GIBCO) supplemented with 10% fetal bovine serum (FBS, GILBCO), 100 U/mL penicillin, and 100 mg/mL streptomycin (Sigma). MG-63 cells were then harvested with a 0.25% trypsin–EDTA solution (Sigma) in phosphate-buffered saline (PBS, pH 7.4). The sample size for cell culture and seeding was $10 \times 10 \text{ mm}^2$, besides that a specific amount of cell culture was kept as the control sample. It is also worth mentioning that the samples were firstly sterilized using medical-grade ethanol for 2 h and then with the help of autoclave using hot steam at $120 \text{ }^\circ\text{C}$ and 1.5 kg/m^3 .

MTT assay

Dimethylthiazol diphenyl tetrazolium bromide (MTT) assay was carried out to assess the proliferation rate of osteoblast cells and samples cytotoxicity. The test which is based on MTT reduction to a formazan dye by living cells, was carried out for 7- and 14-day period [22]. For this purpose, a density of 10^4 cells/mL was added to the culture and then seeded in each of 96-well plates. The plates were then incubated at $37 \text{ }^\circ\text{C}$ in a humidified atmosphere of 5 vol% CO_2 for 24 h. Thereafter, the samples were then placed on MG-63 cells in addition with the pure cell culture as the control sample and then the plates were incubated under the same conditions for 7 and 14 days. MTT solution at a concentration of 5 mg/mL in phosphate-buffered saline (PBS) was added to each well and incubated for another 5 h under the same described conditions. At this stage, the MTT was removed and the converted formazan crystals were dissolved by adding 100 mL of isopropanol solution. After another round of incubation for 15 min, an Elisa microplate reader was used to measure absorbance of converted dye at a wavelength of 570 nm.

Cell morphology

In order to evaluate surface and intrinsic characteristics of each sample for the cells to attach and remain

on, a density of 3×10^4 cells/mL was added to the plates containing samples and then it was incubated for 72 h at $37 \text{ }^\circ\text{C}$ in humidified air containing 5 vol% CO_2 . Subsequently, after cells adhesion was assured, the samples were stabilized by 4% glutaraldehyde buffered in 0.2 M PBS and were then frozen for 24 h. Ultimately the samples were dehydrated by ethanol with varying purities and were coated to undergo SEM evaluations.

Alkaline phosphatase enzyme activity

Alkaline phosphatase, also known as ALP, is an enzyme of the hydrolase family produced by osteoblast cells. This enzyme separates the phosphate groups from other molecules such as proteins, nucleotides, and alkaloids, which in consequence provide an adequate amount of accumulated phosphates and therefore accelerates osteoblasts activities. In case of biomaterials, measuring ALP released in contact with, is an efficient way to assess biomaterials effect on osteoconductivity. For this purpose, MG-63 cells were trypsinated for 7 days and then a density of 5×10^4 cells/mL in 10% fetal calf serum (FCS) were added to each of the wells containing samples. The plate was incubated for 7 days at $37 \text{ }^\circ\text{C}$, and then the cell culture was analyzed using an AUDIT-KIT (Hitachi-911) to measure ALP concentrations.

Results and discussion

Characterization of synthesized hydroxyapatite

XRD pattern of the nanosized HAp powder, shown in Fig. 3, provides diffraction information of the synthesized powder in the range of $2\theta = 20^\circ\text{--}80^\circ$. Phase analysis performed referencing the standard card JCPDS 009-0432 for HAp, revealed the presence of all major peaks of HAp, including the ones at 2θ values of 25.879° , 31.802° , 32.188° , 32.944° , 39.832° , 46.706° and 49.779° . In addition, Table 2 which summarizes the comparative information extracted from XRD analysis, proved the same observation in accordance with the pattern. Likewise, there were no new peaks in the diffracted pattern which infers to high purity of the powder. As a result, XRD analysis can verify the purity and structure of the synthesized powder. On the other hand, SEM images taken of the

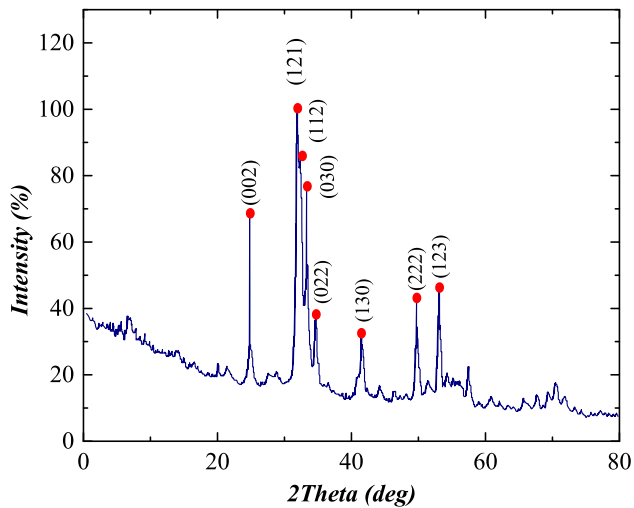


Figure 3 XRD pattern of the synthesized HAP powder with indicated major peaks and their diffraction planes.

powder nanoparticles are shown in Fig. 4. The micrographs infer to the nanorange size for the particles with conformity in both the size and shape distributions, the distinctively separated particles range from 46 to 63 nm as shown in Fig. 4a. Consequently, one can claim that the average particle size of HAP could be estimated as 54 nm. Besides, EDS analysis performed during imaging is also shown in Fig. 4 and proves that Ca/P ratio for the synthesized powder is 1.78 and is in accordance with the required expectations for HAP.

Mechanical properties

Figure 5 illustrates the representative tensile stress–strain curves of the samples. Elastic modulus, yield

strength, tensile strength, i.e., the stress at rupture point and elongation at break obtained from the plots are also comparatively reported in Fig. 5. The mechanical test results are shown numerically in Table 3.

As seen in Fig. 5, elastic modulus, yield strength and tensile strength experience a steady increase with fillers addition, while elongation at break decreased with the addition of fillers. From now on, we focus on elastic modulus, yield strength and elongation to break to analyze the mechanical performance of the materials made. This is due to the fact that in arthroplasty, the implant is not allowed to yield and its plastic deformation beyond yield point is considered failure.

According to Fig. 5, elastic modulus and yield strength of UH sample containing 10 wt% HAP were improved by about 41% and 14%, respectively, compared to those of the neat U sample, which is in agreement with the previous studies [11, 23]. Addition of zirconia to this system further increased these values such that UHZ(10) containing 10 wt% HAP and 10 wt% zirconia has elastic modulus and yield strength of about 70% and 29%, respectively, higher than those of the neat sample. It is interesting to note that this much improvement in mechanical properties of UHMWPE has been previously reported at 40 wt% loading of HAP [11]. Therefore, one may conclude that simultaneous incorporation of HAP and zirconia is a better choice for mechanical properties improvement of UHMWPE in comparison with the use of HAP alone since fewer amount of filler is needed.

Table 2 Diffraction planes, d spacing, position and intensities of the synthesized powder in comparison with the standard card JCPDS 009-0432

Peak number	(hkl)	d (Å)		2θ (°)		I (%)	
		Synthesized powder	Standard card	Synthesized powder	Standard card	Synthesized powder	Standard card
1	(002)	3.4415	3.4450	25.876	25.841	73.04	36.2
2	(121)	2.8115	2.8149	31.802	31.763	100	100
3	(112)	2.7786	2.7808	32.188	32.163	54.00	57.2
4	(030)	2.7166	2.7196	32.944	32.904	63.34	63.5
5	(022)	2.6300	2.6321	34.062	34.003	29.02	22.9
6	(130)	2.2613	2.2630	39.832	39.799	23.35	21.8
7	(222)	1.9432	1.9443	46.706	46.676	28.27	39.9
8	(123)	1.8410	1.8420	49.476	49.449	37.40	34.6

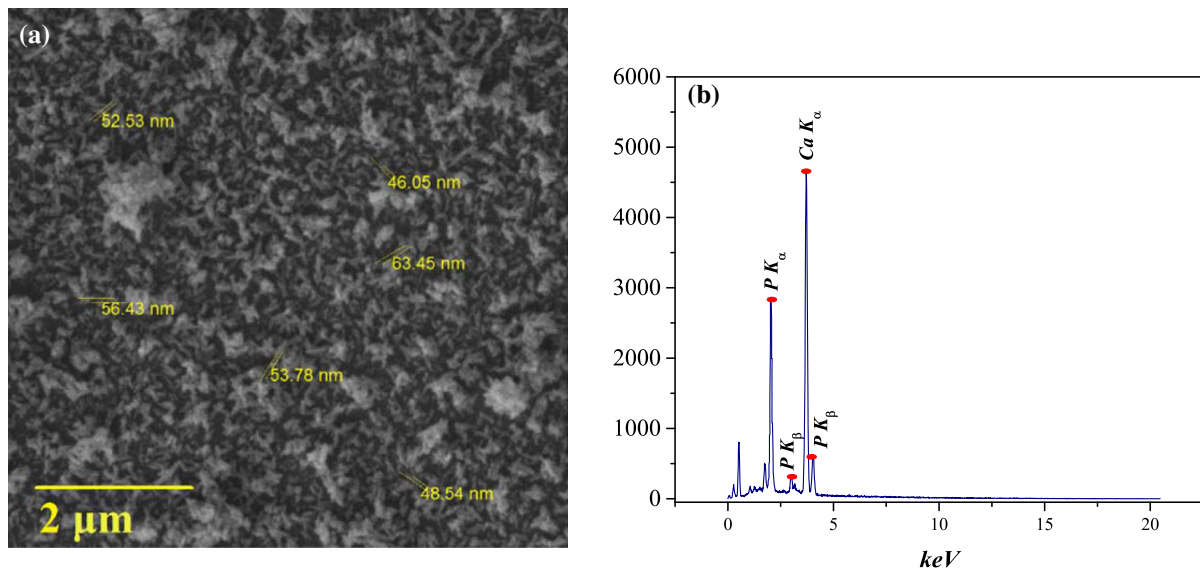


Figure 4 a SEM micrograph of the dispersed HAp powder and its particle sizes and b EDS pattern of the same powder.

Figure 5 also reveals a decreasing effect of filler on the elongation at break where the minimum value is observed in the case of UHZ(10) with 38% lower elongation at break compared to the neat UHMWPE. Although this negative effect of brittle ceramic fillers on the ductile polymer matrix is not negligible, all UHZ series of samples satisfy the required tensile properties for total hip joint replacement. According to the published literature, UHMWPE sockets used in total hip joint replacement should possess yield strength and elongation at break of 19 MPa and 250%, respectively [1]. Figure 5 illustrates that while all UHZ series of samples have high enough yield strength and elongation at break, they have much higher elastic modulus and tensile strength than the neat UHMWPE. Similarly, the achieved tensile properties of the current study are significantly improved compared to that of the single introduction of HAp [11, 23], zirconia [24], and carbon-based fillers [22, 25].

Figure 6 illustrates the microhardness values of the samples tried in this study. As seen, steady increase occurs by addition of fillers. The maximum improvement was observed in the case of UHZ(10) where the microhardness is increased by 84% compared to the neat U sample. The same material is 43% harder than the sample containing 10 wt% HAp (UH). Comparing these results with those reported by other investigators, again, emphasizes the superiority of incorporating HAp-zirconia pair in UHMWPE matrix. Chen et al. [22] observed 15%

increase in microhardness when employed 1 wt% GO. Shirong et al. [26] reported 65% increase in hardness of UHMWPE by adding 30 wt% coral particles. Bodhak et al. [27] were able to increase hardness of their matrix to something close to what found in this study when they incorporated 40 wt% alumina which is double of what used here. Additionally it is also worthy to mention that according to Davis [1], the standard microhardness value for a UHMWPE socket has to be around 6.1 Hv (60 MPa), which qualifies all UHZ series of samples for such applications.

In order to interpret the elevation in mechanical properties, dispersion and distribution state, interfacial properties and microstructural evolution or changes are key factors to evaluate [8, 11, 28]. A homogeneous dispersion, conform distribution and proper interfacial adhesion result in effective stress transfer from matrix to reinforcing particles which leads to eventual improvement in mechanical properties. In addition, it is worthy to mention that due to the high chemical stability of both UHMWPE matrix and ceramic fillers at the operating temperature, no chemical reaction or bonding is expected to occur at the interfacial area [28]. Consequently, it is expected that only the particle encapsulation quality by the polymer matrix, affects the interfacial properties [13, 29]. SEM micrographs, taken from various parts of polished cryogenic fracture surfaces, shown in Fig. 7, were employed to assess dispersion and distribution states as well as interfaces between

Figure 5 **a** Representative tensile stress–strain curves of samples, **b** elastic modulus, **c** yield strength, **d** tensile strength and **e** elongation at breakoff the samples.

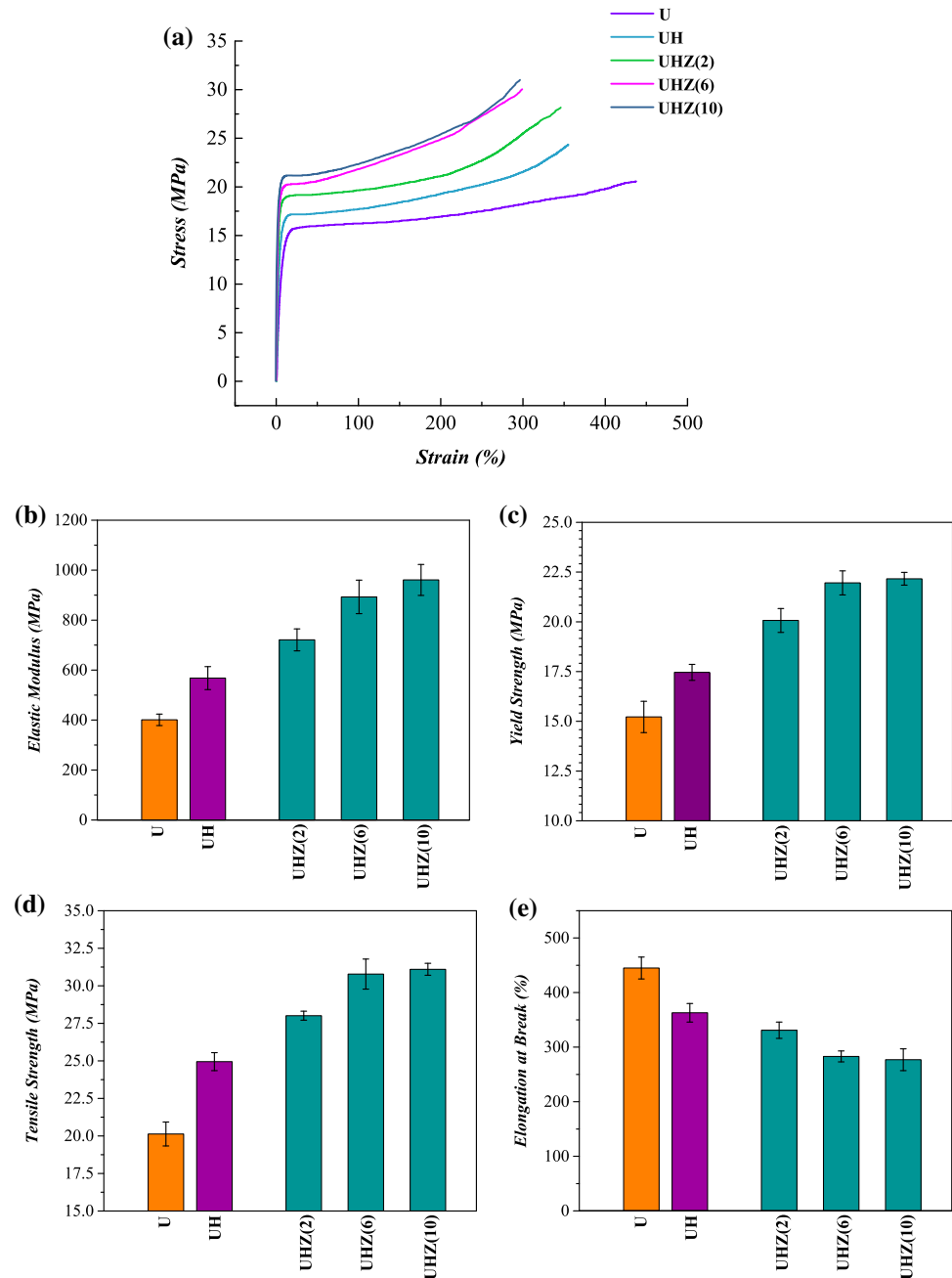


Table 3 Mechanical test results of the samples

Sample name	Tensile properties				Vickers hardness
	Elastic modulus (MPa)	Yield strength (MPa)	Tensile strength (MPa)	Elongation at break (100%)	Hardness (H_v)
U	401 ± 23	15.23 ± 0.7	20.13 ± 0.8	4.42 ± 0.5	5.9 ± 0.3
UH	568 ± 46	17.61 ± 0.4	24.95 ± 0.6	3.61 ± 0.4	7.6 ± 0.2
UHZ(2)	721 ± 44	20.07 ± 0.6	28.01 ± 0.2	3.35 ± 0.4	8.4 ± 0.2
UHZ(6)	893 ± 67	21.95 ± 0.6	30.7 ± 0.3	2.96 ± 0.5	9.8 ± 0.1
UHZ(10)	961 ± 63	22.16 ± 0.3	31.12 ± 0.3	2.83 ± 0.5	10.9 ± 0.1

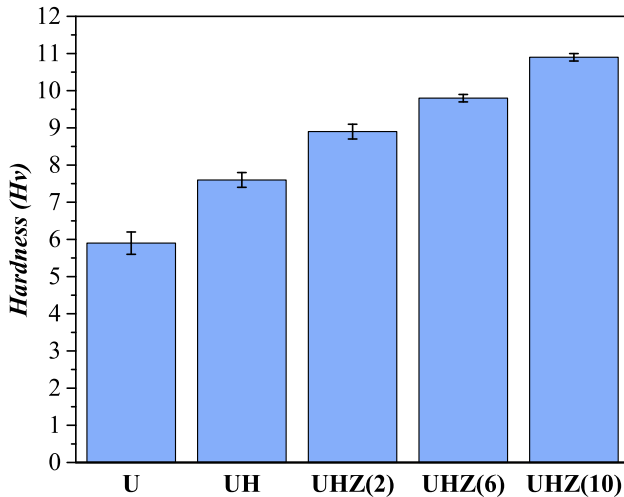


Figure 6 Average Vickers microhardness values of the samples.

reinforcing particles and polymeric matrix where a secondary electron (SE) detector was used to distinguish ceramic particles from matrix. According to Fig. 7a, b taken from the sample UH, where lighter spots marked by circles represent HAp particles, a uniform distribution with little agglomeration was observed. Besides, absence or existence of only a few micropores in the areas surrounding the particles could refer to appropriate polymeric encapsulation which itself results in more efficient load transfer [13, 29]. Similar distribution states and interfacial conditions were also observed in UHZ(6) and UHZ(10) samples as shown in Fig. 7c–f. According to Fig. 7c, e, zirconia nanoparticles which appear brighter than HAp nanoparticles as a result of their larger molecular mass, were homogeneously distributed but were also agglomerated in some areas due to the higher surface energy of nanosized particles which resulted in their tendency to interact more and therefore inevitably agglomerate. In addition, in Fig. 7g, which is taken from sample UHZ(10), EDS analysis pattern carried out on the marked area of the sample is seen which demonstrated the presence of zirconium, calcium and phosphorous elements that are representatives of zirconia and HAp particles. Resultantly, SEM micrographs could approve the appropriate distribution, the integrity of the nanocomposites and the absence of micropores.

Crystallization temperature (T_c) and degree of crystallization (X_c), were evaluated by means of DSC analysis to assess microstructural changes following the introduction of reinforcements to the matrix. Crystallization temperature was measured from the

peak temperature in DSC exothermic plots (Fig. 8) and degree of crystallinity was measured by means of Eq. 2:

$$X_c = \Delta H / (1 - \phi) \Delta H^\circ \quad (2)$$

where ΔH is the apparent enthalpy of fusion per gram of composite, ΔH° is the heat of fusion of a 100% crystalline polyethylene taken as 293 J/g, and ϕ is the weight fraction of the filler in the composites. The results are summarized in Table 4. As seen in this table, both T_c and X_c increased with addition of zirconia, which is an indication of the nucleating effect of zirconia nanoparticles on crystallization and microstructural properties of the matrix. UHMWPE, as a semi-crystalline polymer, would present elevated mechanical properties when the number, concentration or thickness of crystalline areas are increased, which eventually increase the degree and temperature of crystallinity [9]. Therefore, nucleating effect of reinforcement and the enhanced crystalline structure of the matrix, might be considered as another reason for mechanical properties improvement in these composites.

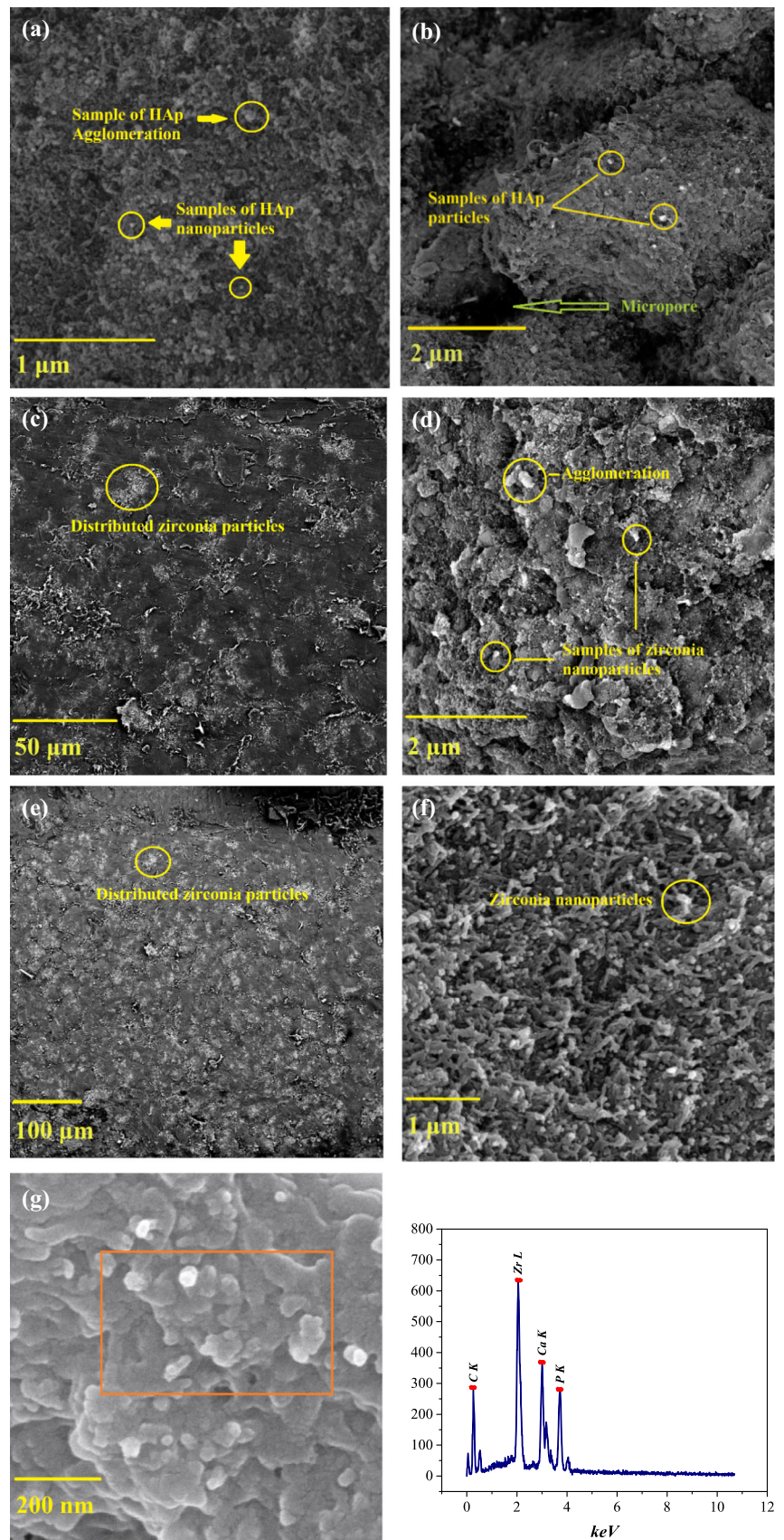
Wear properties

Figure 9 illustrates comparative coefficient of friction (COF) plots of each nanocomposite in a total sliding distance of 1000 m, which proves that frictional interactions between the indenter and the samples decreased with the introduction of the fillers, as the fluctuation of the patterns visibly decreased with the addition of the fillers. In addition, Fig. 9 shows optical microscope images taken of wear widths on each sample, which proves the decrease in wear width with increasing zirconia content: as for UHZ(10) sample, the wear width decreased by 67% and 64% compared to the neat and UH samples, respectively.

Statistically, Table 5 summarizes the tribological data extracted from wear test including mean COF and normalized wear rates as indicators of wear behavior of the samples. These two tribological factors are comparatively presented in Fig. 10.

As seen, the reduction in both wear rates and coefficients of friction indicates the efficiency of HAp-zirconia simultaneous incorporation to improve wear resistance, i.e., addition of 6 wt% and 10 wt% zirconia to the UHMWPE/HAp (UH) sample resulted in 57%

Figure 7 SEM micrographs at different magnifications taken from cryogenic fracture surface of **a, b** UH, **c, d** UHZ(6), **e, f** UHZ(10) along with **g** SEM and EDS taken from UHZ(10).



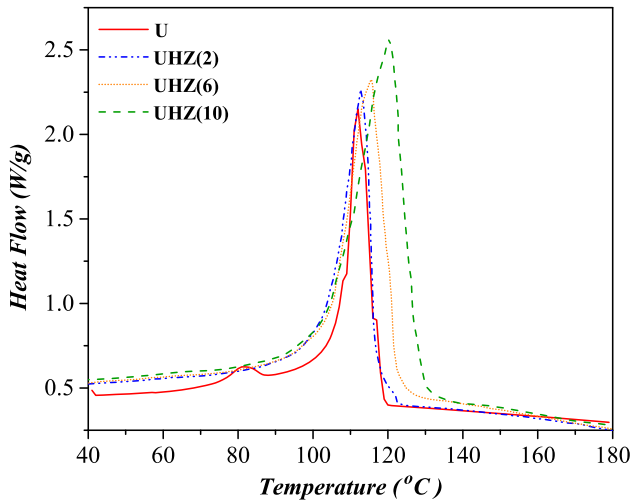


Figure 8 Exothermic DSC plots of the neat U and UHZ series samples.

Table 4 Crystallization degree (X_c) and temperature (T_c) taken from DSC plots

	Crystallization degree (wt%)	Crystallization Temperature (°C)
U	42	115.2
UHZ(2)	46.5	117.8
UHZ(6)	48.3	119.1
UHZ(10)	50.8	120.2

and 61% reduction in COF, respectively. Similarly, the wear rate decreased by 87 and 88% when 6 and 10 wt% zirconia was added to the UH sample, respectively.

Comparing the results of the current study with those of other researchers who incorporated zirconia in UHMWPE illustrates again the superiority of simultaneous introduction of HAp and zirconia into the matrix. Park et al. [13], for example, employed up to 43 wt% of zirconia into UHMWPE and the maximum reduction in COF and wear rate they observed was 10 and 25%, respectively. Besides, when compared to studies evaluating the effect of kaolin [14], HAp [30], alumina [31], zeolite [32], and some other inorganic fillers briefly reviewed in Maculevė’s study [15] on wear properties, zirconia-HAp simultaneous incorporation used in the current research remarkably increased wear resistance of the eventual material at much lower filler contents.

In order to justify the results obtained in the current study, one may propose that in the hybrid nanocomposite, HAp and zirconia particles would keep the soft polymer from the frictional indenter and reduce the stress exerted by the counterface, a phenomenon that is known as load-carrying capacity [32]. However, this would only occur if the frictional load is effectively transferred from matrix to

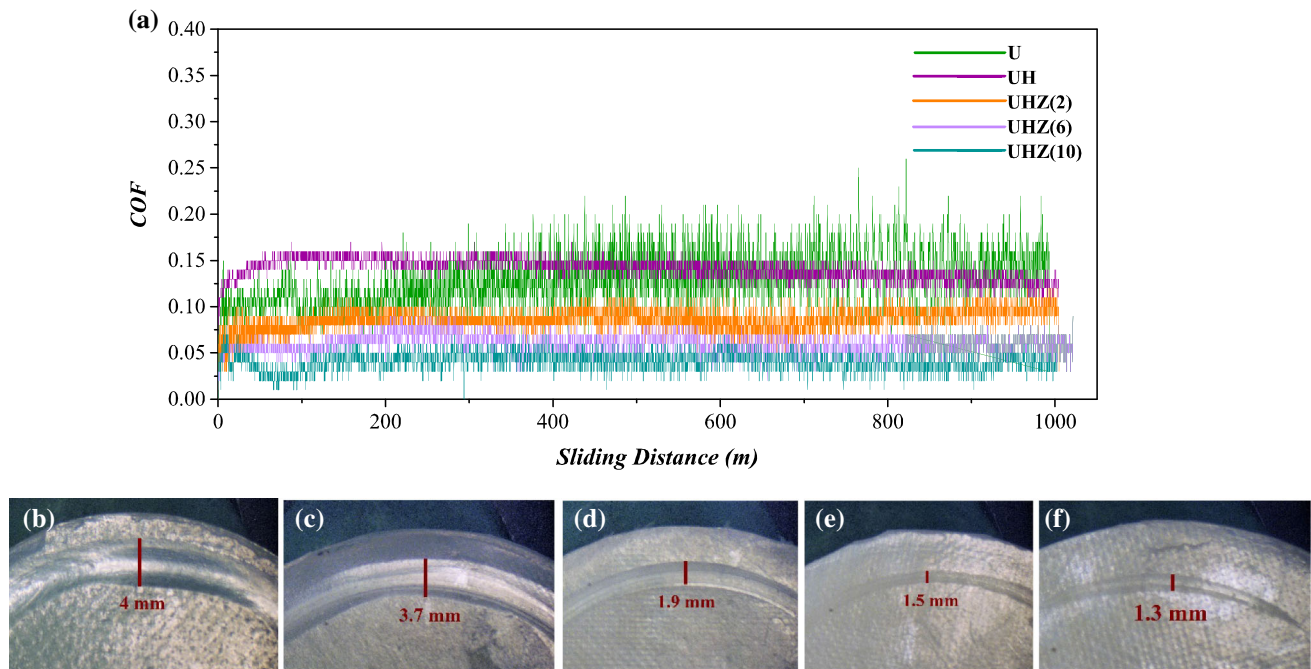
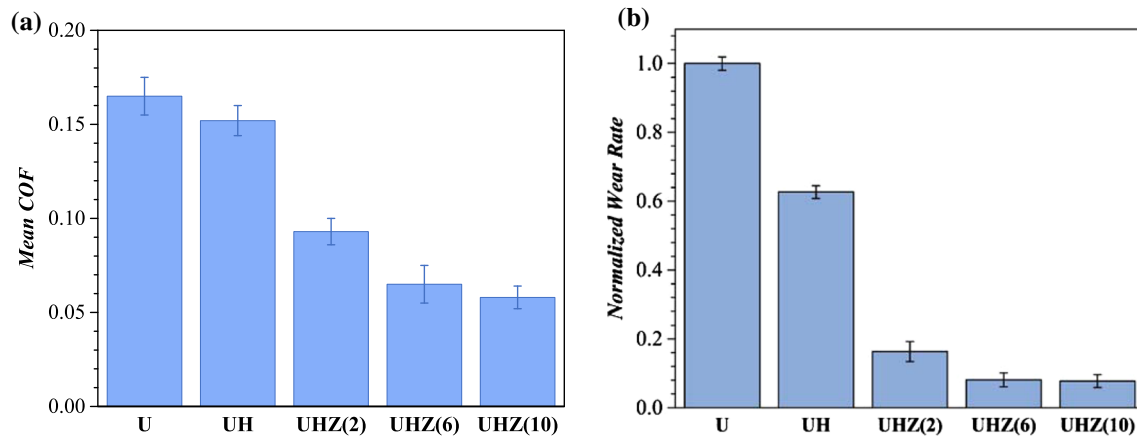


Figure 9 a COF of the samples as a function of sliding distance throughout the wear test and OM images of wear width of a U, b UH, c UHZ(2), d UHZ(6) and e UHZ(10) samples.

Table 5 Tribological results extracted from wear test analysis

Sample name	COF (%)	Weight reduction (mg)	Density (Kg/m ³)	Wear rate (m ² /N)	Normalized wear rate
U	0.165	1	8.375	0.0199	1
UH	0.152	0.7	9.336	0.0124	0.623
UHZ(2)	0.093	0.2	10.250	0.00325	0.163
UHZ(6)	0.065	0.1	10.289	0.00161	0.080
UHZ(10)	0.058	0.1	10.780	0.00154	0.077

**Figure 10** Calculated **a** mean coefficients of friction and **b** normalized wear rates of samples.

reinforcing particles, which itself is affected by the dispersion state. Homogeneous contact between the counterfriction surfaces, resulted from homogeneously dispersed particles, enables the filler particles to play their reinforcing role in eventual improvement in wear resistance. Therefore, the resulted wear resistance improvement could be attributed to the effective processing and manufacturing technique used in this study which led to uniformly distributed zirconia and HAp nanoparticles.

Besides, according to Liu et al. [33], ploughing and adhesive forces are the two main factors taking part in wear process in the presence of an appropriate interfacing, which is also affected by the quality and the degree of dispersion. Therefore, a homogeneously distributed nanostructure, adhesive forces would weaken the ploughing ones and hinder the wearing process. In addition, adhesive forces are also strengthened when samples exhibit higher elastic modulus and hardness. Thereupon, as only a few clusters and agglomerations are observed in Fig. 8, one could also relate the wear resistance improvement to elaborated adhesive forces when intrinsically hard zirconia-HAp nanoparticles act as load carriers.

Additionally, Vickers testing results presented in the previous section, were also in accordance to wear testing results, where the increase in hardness could be the reason for adhesive forces strengthening and eventually increasing wear resistance.

Although there are numerous references which consider no significant relation between the crystalline structure of the polymeric matrix and wear resistance [34], according to some others, whatever increases the crystalline degree, elastic modulus and hardness would eventually increase wear resistance [35–37]. Therefore, another possible reason of the increased wear resistance could be the nucleating effect of zirconia nanoparticles on UHMWPE chains, which was discussed in the previous section by means of the DSC results shown in Fig. 8 and Table 4.

As a sequel, wear rate and COF in UHZ(10) sample were reduced by 88 and 61%, respectively, when compared to the neat U sample. Therefore, it can be concluded that the wear debris, as the main reason of osteolysis and implant failure, can be eliminated as much as possible in a hybrid nanocomposite containing HAp and zirconia particles.

Biological properties

Biological behavior of the samples was investigated through MTT assay, cell morphology and alkaline phosphatase enzyme level. According to MTT assay results, shown in Fig. 11a, all samples have proven to make no reverse or toxic effect in a period of 7 and 14 days, if the index of appropriate viability considered as 85% [38]. Increasing viability in UH sample with respect to the control and U cultures is due to the addition of hydroxyapatite as a bioactive material. Relative survivability of the osteoblast MG-63 cells even increased slightly with the rising content of zirconia, which would strengthen the idea of zirconia bioinertness, as it was previously reported [16]. Accordingly, MTT assay indicated that all samples especially the ones containing zirconia, were completely biocompatible and showed no negative effect on the survivability of MG-63 cells.

The amount of alkaline phosphatase enzyme concentration in the cultures containing samples for 7 days were measured to evaluate how well osteoblast MG-63 cells could grow and multiply in presence of samples. As shown in Fig. 11b, the ALP enzyme for U sample reduced when compared to the control culture, which may have happened due to lack of osteoconductivity of UHMWPE as a chemically inert material. While by adding hydroxyapatite as an osteoconductive material with a structure similar to the mineral component of natural bone, the ALP enzyme rose slightly. At the same time, in samples containing zirconia, the amount of ALP concentration increased almost significantly especially in UHZ(6) and UHZ(10). In consequence, the

reason could be attributed to reported osteoconductive ability of zirconia and alumina which was observed in previous studies [16].

In order to have a full assessment of in vitro biological behavior of the samples, cell morphologies were also surveyed with the details described in previous sections. Cell attachment quality and quantity, which is related to samples intrinsic and surface properties, determines how well cells could attach, proliferate and multiply with specific surface conditions and consequently is an index of surface suitability for the cells to be attached to and to survive [22]. According to Fig. 12a, which shows cell attachment on the surface of the U sample, MG-63 cells were scattered all over the surface with only a few ligands attached to the surface which are marked by circles. While in UH sample in Fig. 12b, cells have covered the surface with only a few spherical cells as a sign of insufficient attachment. Moreover, although there was an almost homogeneous cell coverage on the surface of UHZ(2) sample shown in Fig. 12c, the presence of spherical cells and pseudopods over the surface was also observed. Besides, there were also cell ligands adhered to the surface in some areas.

On the contrary, in UHZ(6) and UHZ(10), as shown in Fig. 12d, e, the surfaces were almost entirely covered with cells with no sign of spherical cells which demonstrated an almost ideal surface for the cells to attach on and multiply, meaning that adding zirconia surprisingly increased biological compatibility of the samples and provided a better substrate for metabolic interactions of the cells.

Determinately, according to the three biological tests carried out, it can be concluded that zirconia-

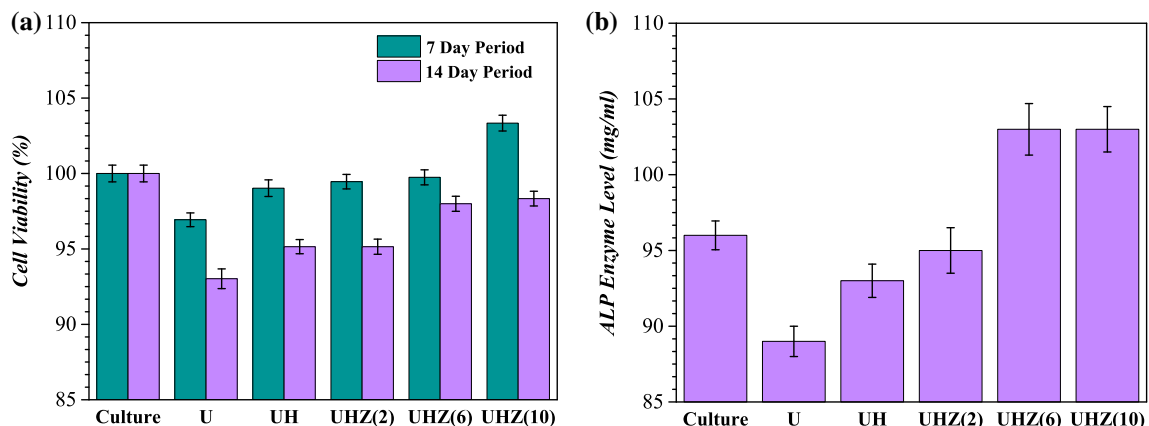
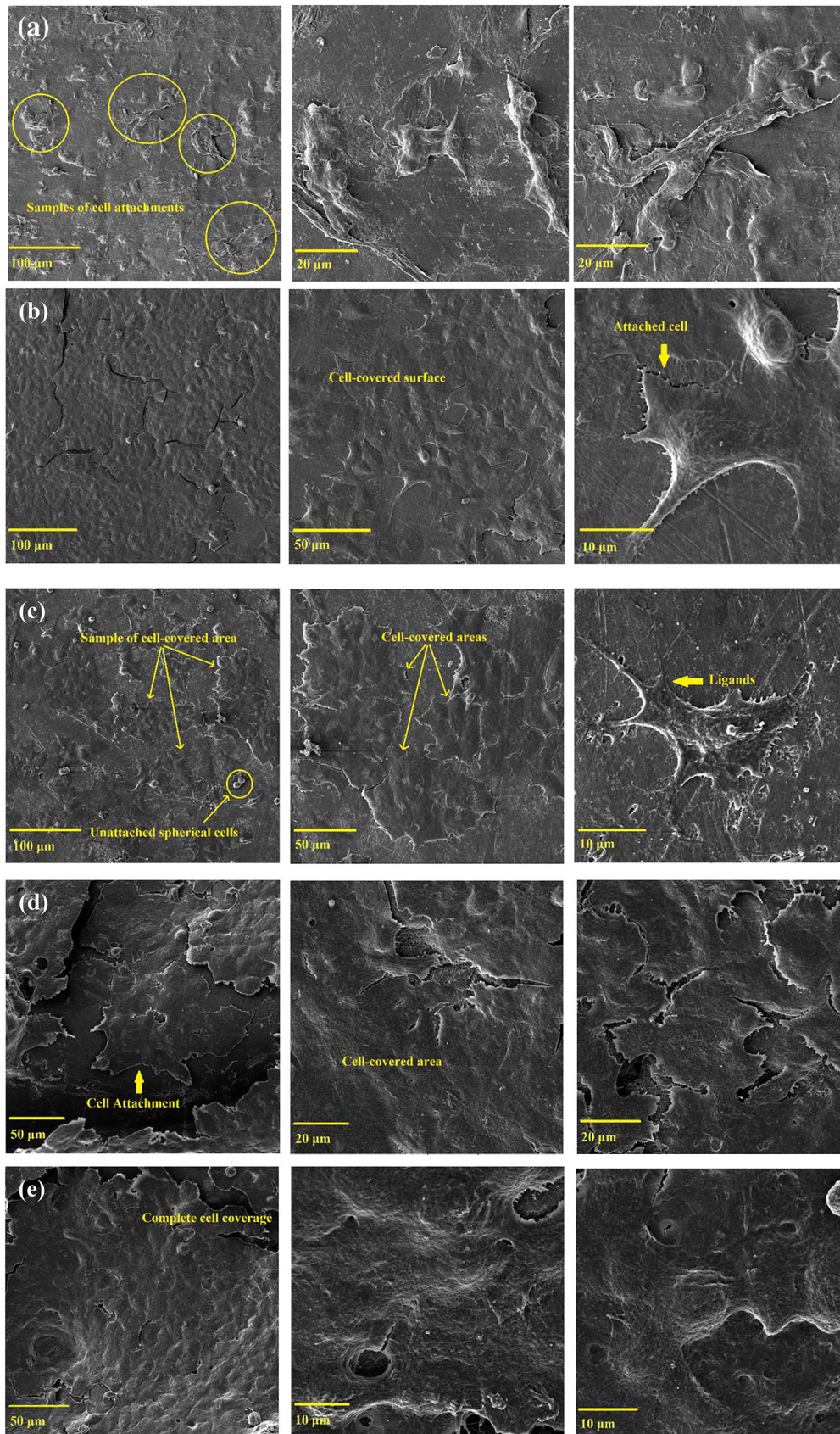


Figure 11 **a** MTT assay test results to evaluate samples biocompatibility in 7 and 14 day periods and **b** alkaline phosphatase (ALP) enzyme concentrations in presence of the cultured samples after 7 days.



◀ **Figure 12** SEM images at different magnifications of cell morphology on **a** U, **b** UH, **c** UHZ(2), **d** UHZ(6) and **e** UHZ(10).

HAp simultaneous incorporation has provided more appropriate environments for the MG-63 osteoblast cells to survive and perform their vital metabolic reactions. Therefore, it would ultimately mean that zirconia containing samples, especially UHZ(6) and UHZ(10), would exhibit better *in vitro* biocompatibility, osteocell formation and growth than HAp alone. In addition, although zirconia is known as a bio-inert material, it has demonstrated osteoconductivity in this study. *In vitro* interaction of zirconia and alumina with osteoblast cells has been referenced in a biocompatibility point of view for years [16, 38]. Bächle et al. [39] found out that zirconia nanoparticles showed good surface attachment and proliferation of the CAL-72 osteoblast-like cells which indicated that zirconia demonstrated an osteoconductive capability through providing a secreted extracellular matrix (ESM), where cells were able to adhere, grow and spread more easily. In addition, zirconia involves in short-term events like physicochemical linkages between cells and materials involving ionic forces and van der Waals forces. In the adhesion phase of the cells, other biological molecules like extracellular matrix proteins, cell membrane proteins, and cytoskeleton proteins interact together, giving the conclusion that the more osteoconductive the material is, the better attachment would occur [39]. They have also claimed that the reason of rising alkaline phosphatase level with increasing zirconia content was similarly related to the same capability which would facilitate osteoenzymes release and therefore facilitates bone tissue formation in contact with the material. According to Josset et al. [40], the ability of zirconia and alumina to facilitate migration and colonization of osteoblast cells was considered as the reason to high alkaline phosphatase activity and cell proliferation along with more than 90% viability cultured on these ceramics. They have also reported capabilities such as acceleration of infrastructural proteins synthesis in presence of zirconia which resulted in elaborating extracellular molecules preceding mineral deposition, a sequence of events leading to bone formation. Aboushelib et al. [41], studied viability of human osteoblasts on zirconia nanoporous structures and discovered the same

results which approved the osteoconductivity of zirconia and its role on osteoformation and biocompatibility of the final implants. According to Yoo et al. [42], oxidative stress caused by release of free radicals following the sterilization or other processes, is the main reason of cells death. Thereafter, the addition of zirconia nanoparticles might increase stability of UHMWPE and decrease the number of free radicals released into the culture which in consequence increase the survivability and growth of the cells. Eventually, inherent osteoconductivity of zirconia along with its capability to facilitate protein synthesis and ECM stabilization are believed to result in excellent biological properties that were observed in this study, making it one of the best candidates to be used as bone tissue implants. It has also demonstrated better biological properties than the commonly used hydroxyapatite which may bring up the idea of a prospective replacement for the current commercially used hydroxyapatite reinforced nanocomposites.

It is worthful to mention that the results of the current study are superior than works done by researchers, for instance, the data reported by various scientists [15], indicate the same value for cell viability by adding at least 50 wt% of hydroxyapatite to UHMWPE matrix, while the results of the current study reveal that the same amount could be achieved by adding less than half the proportion used in the mentioned work. On the other hand, introducing zirconia as a propitious biocompatible material, which was only briefly worked on as a candidate to eliminate the setbacks of UHMWPE liners [24, 27, 40, 43], has resulted in much improved cell adhesion even than HAp and carbonous materials such as CNT, graphene, and graphene oxide [44].

Conclusion

As an implant material, liners of the total hip joint replacement are expected to meet the standards in the fields of wear resistance, mechanical properties and biological interactions with the surrounding tissue. Therefore, zirconia and hydroxyapatite were chosen as potential reinforcements for the conventional UHMWPE liners to elevate its required properties. A simple liquid-phase mixing and ultrasonication were chosen followed by hot pressing to obtain the final nanocomposite samples. The

addition of zirconia to HAp significantly improved wear resistance in comparison with hydroxyapatite alone and furthermore eliminated the concern of wear debris and adverse biological responses caused by osteolysis. Zirconia-HAp simultaneous incorporation was also able to elevate mechanical properties when compared to hydroxyapatite which did not prove to be an appropriate reinforcement to meet the required yield strength. Zirconia have also demonstrated exceptional biological responses in presence of MG-63 osteoblast cell cultures with making no cytotoxicity and high alkaline phosphatase activity along with fully spread osteocells. Therefore, the present study has evaluated zirconia-HAp simultaneous incorporation as a promising material to overcome the shortcoming of the conventionally used UHMWPE to improve its insufficient mechanical, tribological, and biological properties as an implant liner. Besides, the reduction of reinforcement usage to less than half of the conventional values used in other studies, and surpassing the embellishment in results reported by those studies, are also another important achievements of the current research.

Data availability

The raw/processed data required to reproduce these findings cannot be shared at this time due to technical or time limitations.

Compliance with ethical standards

Conflict of interest The first two authors have worked on the project at Polymeric Materials Research Group (PMRG) at the Department of Materials Science and Engineering of Sharif University of Technology. The project was supervised by Dr. Reza Bagheri and Dr. Mohammad Ali Faghihi Sani, professors at the same department. The authors certify that they have NO affiliations with or involvement in any other institute, organization or entity with any financial interest.

References

- [1] Davis J (2003) Handbook of materials for medical devices. ASM Int. pp 205–216. <https://doi.org/10.1361/hmmd2003p001>
- [2] Shin H, Jo S, Mikos AG (2003) Biomimetic materials for tissue engineering. *Biomaterials* 24:4353–4364. [https://doi.org/10.1016/S0142-9612\(03\)00339-9](https://doi.org/10.1016/S0142-9612(03)00339-9)
- [3] Agrawal CM (1998) Reconstructing the human body using biomaterials. *JOM J Miner Met Mater Soc* 50:31–35
- [4] Katti KS (2004) Biomaterials in total joint replacement. *Colloids Surf B: Biointerfaces* 39:133–142. <https://doi.org/10.1016/j.colsurfb.2003.12.002>
- [5] Modjarrad K, Ebnesajjad S (2014) Handbook of polymer applications in medicine and medical devices
- [6] Kurtz SM (2009) UHMWPE biomaterials handbook: ultra high molecular weight polyethylene in total joint replacement and medical devices. Academic Press, Cambridge, MA, US
- [7] Ingham E, Fisher J (2000) Biological reactions to wear debris in total joint replacement. *Proc Inst Mech Eng Part H J Eng Med* 214:21–37. <https://doi.org/10.1243/0954411001535219>
- [8] Lahiri D, Dua R, Zhang C, De Socarraz-Novoa I, Bhat A, Ramaswamy S, Agarwal A (2012) Graphene nanoplatelet-induced strengthening of ultrahigh molecular weight polyethylene and biocompatibility in vitro. *ACS Appl Mater Interfaces* 4:2234–2241. <https://doi.org/10.1021/am300244s>
- [9] Brach del Prever EM, Bistolfi A, Bracco P, Costa L (2009) UHMWPE for arthroplasty: Past or future? *J Orthop Traumatol* 10:1–8. <https://doi.org/10.1007/s10195-008-0038-y>
- [10] Kurtz SM, Hozack W, Turner J, Purtill J, MacDonald D, Sharkey P, Parvizi J, Manley M, Rothman R (2005) Mechanical properties of retrieved highly cross-linked crossfire liners after short-term implantation. *J Arthroplasty* 20:840–849. <https://doi.org/10.1016/j.arth.2005.07.015>
- [11] Mirsalehi SA, Sattari M, Khavandi A, Mirdamadi S, Naimi-Jamal MR (2015) Tensile and biocompatibility properties of synthesized nano-hydroxyapatite reinforced ultrahigh molecular weight polyethylene nanocomposite. *J Compos Mater* 177:17–20. <https://doi.org/10.1016/j.matlet.2016.04.072>
- [12] Fang L, Leng Y, Gao P (2006) Processing and mechanical properties of HA/UHMWPE nanocomposites. *Biomaterials* 27:3701–3707. <https://doi.org/10.1016/j.biomaterials.2006.02.023>
- [13] Park HJ, Kwak SY, Kwak S (2005) Wear-resistant ultra high molecular weight polyethylene/zirconia composites prepared by in situ ziegler-natta polymerization. *Macromol Chem Phys* 206:945–950. <https://doi.org/10.1002/macp.200400350>
- [14] Guofang G, Huayong Y, Xin F (2004) Tribological properties of kaolin filled UHMWPE composites in unlubricated sliding. *Wear* 256:88–94. [https://doi.org/10.1016/S0043-1648\(03\)00394-6](https://doi.org/10.1016/S0043-1648(03)00394-6)

- [15] Macuvele DLP, Nones J, Matsinhe JV, Lima MM, Soares C, Fiori MA, Riella HG (2017) Advances in ultra high molecular weight polyethylene/hydroxyapatite composites for biomedical applications: a brief review. *Mater Sci Eng C* 76:1248–1262. <https://doi.org/10.1016/j.msec.2017.02.070>
- [16] Hisbergues M, Vendeville S, Vendeville P (2009) Review zirconia: established facts and perspectives for a biomaterial in dental implantology. *J Biomed Mater Res Part B Appl Biomater* 88:519–529. <https://doi.org/10.1002/jbm.b.31147>
- [17] Tai Z, Chen Y, An Y, Yan X, Xue Q (2012) Tribological behavior of UHMWPE reinforced with graphene oxide nanosheets. *Tribol Lett* 46:55–63. <https://doi.org/10.1007/s11249-012-9919-6>
- [18] Visco A, Yousef S, Galtieri G, Nocita D, Pistone A, Njuguna J (2016) Thermal mechanical and rheological behaviors of nanocomposites based on UHMWPE/paraffin oil/carbon nanofiller obtained by using different dispersion techniques. *JOM* 68:1078–1089. <https://doi.org/10.1007/s11837-016-1845-x>
- [19] Feng W, Mu-sen L, Yu-peng L, Yong-xin Q (2005) A simple sol–gel technique for preparing hydroxyapatite nanopowders. *Mater Lett* 59:916–919. <https://doi.org/10.1016/j.matlet.2004.08.041>
- [20] Maksimkin AV, Kaloshkin SD, Kaloshkina MS, Gorshenkov MV, Tcherdyntsev VV, Ergin KS, Shchetinin IV (2012) Ultra-high molecular weight polyethylene reinforced with multi-walled carbon nanotubes: fabrication method and properties. *J Alloys Compd* 536:S538–S540. <https://doi.org/10.1016/j.jallcom.2012.01.151>
- [21] Kang X, Zhang W, Yang C (2016) Mechanical properties study of micro- and nano-hydroxyapatite reinforced ultra-high molecular weight polyethylene composites. *J Appl Polym Sci* 133:1–9. <https://doi.org/10.1002/app.42869>
- [22] Chen Y, Qi Y, Tai Z, Yan X, Zhu F, Xue Q (2012) Preparation, mechanical properties and biocompatibility of graphene oxide/ultra-high molecular weight polyethylene composites. *Eur Polym J* 48:1026–1033. <https://doi.org/10.1016/j.eurpolymj.2012.03.011>
- [23] Liu J-L, Zhu Y-Y, Wang Q-L, Ge S-R (2008) Biotribological behavior of ultra high molecular weight polyethylene composites containing bovine bone hydroxyapatite. *J China Univ Min Technol* 18:606–612
- [24] Patel AK, Trivedi P, Balani K (2016) Carbon nanotube functionalization decreases osteogenic differentiation in aluminum oxide reinforced ultrahigh molecular weight polyethylene. *ACS Biomater Sci Eng* 2:1242–1256. <https://doi.org/10.1021/acsbiomaterials.6b00154>
- [25] Ruan SL, Gao P, Yang XG, Yu TX (2003) Toughening high performance ultrahigh molecular weight polyethylene using multiwalled carbon nanotubes. *Polymer* 44:5643–5654. [https://doi.org/10.1016/S0032-3861\(03\)00628-1](https://doi.org/10.1016/S0032-3861(03)00628-1)
- [26] Ge S, Wang S, Huang X (2009) Increasing the wear resistance of UHMWPE acetabular cups by adding natural biocompatible particles. *Wear* 267:770–776
- [27] Bodhak S, Nath S, Basu B (2009) Friction and wear properties of novel HDPE–HAP–Al₂O₃ biocomposites against alumina counterface. *J Biomater Appl* 23:407–433. <https://doi.org/10.1177/0885328208090012>
- [28] Gupta A, Tripathi G, Lahiri D, Balani K (2013) Compression molded ultra high molecular weight polyethylene-hydroxyapatite-aluminum oxide-carbon nanotube hybrid composites for hard tissue replacement. *J Mater Sci Technol* 29:514–522. <https://doi.org/10.1016/j.jmst.2013.03.010>
- [29] Puértolas JA, Kurtz SM (2014) Evaluation of carbon nanotubes and graphene as reinforcements for UHMWPE-based composites in arthroplastic applications: a review. *J Mech Behav Biomed Mater* 39:129–145. <https://doi.org/10.1016/j.jmbbm.2014.06.013>
- [30] Mirsalehi SA, Khavandi A, Mirdamadi S, Naimi-Jamal MR, Kalantari SM (2015) Nanomechanical and tribological behavior of hydroxyapatite reinforced ultrahigh molecular weight polyethylene nanocomposites for biomedical applications. *J Appl Polym Sci* 132:1–11. <https://doi.org/10.1002/app.42052>
- [31] Xiong DS, Lin JM, Fan DL (2006) Wear properties of nano-Al₂O₃/UHMWPE composites irradiated by gamma ray against a CoCrMo alloy. *Biomed Mater* 1:175–179. <https://doi.org/10.1088/1748-6041/1/3/013>
- [32] Chang BP, Akil HM, Nasir RM (2013) Mechanical and tribological properties of zeolite-reinforced UHMWPE composite for implant application. *Procedia Eng* 68:88–94. <https://doi.org/10.1016/j.proeng.2013.12.152>
- [33] Liu T, Eyley A, Zhong WH (2016) Simultaneous improvements in wear resistance and mechanical properties of UHMWPE nanocomposite fabricated via a facile approach. *Mater Lett* 177:17–20. <https://doi.org/10.1016/j.matlet.2016.04.072>
- [34] Farrar DF, Brain A (1997) The microstructure of ultra-high molecular weight polyethylene used in total joint replacements. *Biomaterials* 18:1677–1685. [https://doi.org/10.1016/S0142-9612\(97\)00143-9](https://doi.org/10.1016/S0142-9612(97)00143-9)
- [35] Wang YQ, Li J (1999) Sliding wear behavior and mechanism of ultra-high molecular weight polyethylene. *Mater Sci Eng A* 266:155–160. [https://doi.org/10.1016/S0921-5093\(99\)00040-4](https://doi.org/10.1016/S0921-5093(99)00040-4)
- [36] Bahrami H, Ramazani SA, Shafiee M, Kheradmand A (2016) Preparation and investigation of tribological properties of ultra-high molecular weight polyethylene (UHMWPE)/graphene oxide. *Polym Adv Technol* 27:1172–1178

- [37] Chih A, Ansón-Casaos A, Puértolas JA (2017) Frictional and mechanical behavior of graphene/UHMWPE composite coatings. *Tribol Int* 116:295–302. <https://doi.org/10.1016/j.triboint.2017.07.027>
- [38] Granchi D, Ciapetti G, Amato I, Pagani S, Cenni E, Savarino L, Avnet S (2004) The influence of alumina and ultra-high molecular weight polyethylene particles on osteoblast-osteoclast cooperation. *Biomaterials* 25:4037–4045. <https://doi.org/10.1016/j.biomaterials.2003.10.100>
- [39] Bächle M, Butz F, Hübner U, Bakaliniš E, Kohal RJ (2007) Behavior of CAL72 osteoblast-like cells cultured on zirconia ceramics with different surface topographies. *Clin Oral Implants Res* 18:53–59
- [40] Josset Y, OumHamed Z, Zarrinpour A, Lorenzato M, Adnet J-J, Laurent-Maquin D (1999) In vitro reactions of human osteoblasts in culture with zirconia and alumina ceramics. *J Biomed Mater Res* 47:481–493
- [41] Aboushelib MN, Osman E, Jansen I, Everts V, Feilzer AJ (2013) Influence of a nanoporous zirconia implant surface of on cell viability of human osteoblasts. *J Prosthodont* 22:190–195. <https://doi.org/10.1111/j.1532-849X.2012.00920.x>
- [42] Yoo K-D, Kim G-H, Il Noh D, Jang JW, Shim YB, Chun HJ (2013) In vitro evaluation of UHMWPE/zirconia composite using human peripheral blood mononuclear cells. *Macromol Res* 21:108–113. <https://doi.org/10.1007/s13233-013-1055-0>
- [43] Sadi AY, Homaeigohar SSH, Khavandi AR, Javadpour J (2004) The effect of partially stabilized zirconia on the mechanical properties of the hydroxyapatite \pm polyethylene composites. *Mater Sci* 5:853–858
- [44] Pinto AM, Gonçalves IC, Magalhães FD (2013) Graphene-based materials biocompatibility: a review. *Colloids Surf B Biointerfaces* 111:188–202. <https://doi.org/10.1016/j.colsurfb.2013.05.022>